Vector boson excitations near deconfined quantum critical points

Yejin Huh,[*] Philipp Strack, and Subir Sachdev
Department of Physics, Harvard University, Cambridge MA 02138
(Dated: July 29, 2013)

We show that the Néel states of two-dimensional antiferromagnets have low energy vector boson excitations in the vicinity of deconfined quantum critical points. We compute the universal damping of these excitations arising from spin-wave emission. Detection of such a vector boson will demonstrate the existence of emergent topological gauge excitations in a quantum spin system.

Quantum spin systems are expected to display ground states with novel fractionalized and topological gauge excitations which have no analogs in the band insulators of Bloch theory [1]. The theoretical arguments for the existence of such excitations are convincing, but, so far, the excitations have not been detected unambiguously in any experiment, or even in numerical studies of semi-realistic model systems in two spatial dimensions. In experiments, the best candidate so far is the kagome antiferromagnet, and its neutron scattering spectrum displays strong evidence for fractionalization [2], but the specific excitations have not been identified. In numerics, there has been positive evidence for exotic physics in the topological entanglement entropy of the kagome antiferromagnet [3, 4], but this does not directly identify the excitation spectrum. Sandvik [5] has obtained convincing evidence of an emergent U(1) symmetry near the quantum critical point of a spin system, and this is strong, but indirect, evidence of an emergent, topological gauge excitation of a deconfined quantum critical point [6]; however, this does not yield any information on the excitation spectrum of the gauge boson.

In this paper we propose that the antiferromagnetically ordered (*i.e.* Néel) phase of a quantum spin system near a deconfined quantum critical point has an emergent vector boson excitation which should be detectable in numerical studies, and possibly eventually in experiments. This vector boson is the analog of the *W* and *Z* vector bosons of the standard model of particle physics, and is similarly a characteristic signature of the gauge structure of the underlying theory. In two spatial dimensions, the vector boson is universally damped by emissions of multiple spin-wave (*i.e.* Goldstone boson) excitations of the Néel phase, and the present paper will provide a quantitative computation of this damping. The Néel phase also has a universally damped Higgs excitation [7], and this mode has recently been detected in experiments [8] and numerics [9, 10] near a conventional quantum critical point. We argue here that similar methods can allow positive identification of a vector boson excitation in the Néel phase near a deconfined quantum critical point. Note that, while the Higgs mode is present for both conventional and deconfined critical points, the vector boson mode appears only in the latter case.

We note that there is a debate [11–19] in the literature of whether the gauge theory of the antiferromagnet ultimately describes a second-order quantum phase transition in antiferromagnets with a global SU(2) spin rotation symmetry. Our method of detecting the vector boson sidesteps this delicate issue, because the vector boson should exist even if the transition out of the Néel phase is weakly first-order. Its observation would be a direct signature that the theory of deconfined criticality with emergent gauge excitations describes the spectrum of the antiferromagnet at low energies.

For quantum antiferromagents with SU(N) global symmetry, the deconfined critical theory [6, 20] is the CP^{N-1} field theory of relativistic complex scalars ('spinons') z_α ($\alpha = 1 \ldots N$) minimally coupled to a U(1) gauge field A_μ with partition function $Z = \int \mathcal{D}z_\alpha \mathcal{D}\lambda \mathcal{D}A_\mu e^{-\mathcal{S}}$ with

$$\mathcal{S} = \int_x \left[\frac{N}{g} |(\partial_\mu - iA_\mu)z_\alpha|^2 + i\lambda(|z_\alpha|^2 - 1) \right] , \qquad (1)$$

where the integration is over 2+1 dimensional space and (imaginary) time, and λ is a Lagrange multiplier which implements the constraint $\sum_{\alpha=1}^{N} |z_\alpha|^2 = 1$. For $N = 2$, the Néel order parameter, $\mathbf{n}(\mathbf{x})$, is related to the spinons via

$$\mathbf{n} = z_\alpha^* \, \boldsymbol{\sigma}_{\alpha\beta} \, z_\beta , \qquad (2)$$

where $\boldsymbol{\sigma}$ is a vector of Pauli matrices.

We are interested here in the spectrum of A_μ excitations in the Néel phase at zero temperature, which appears for $g < g_c$ with $\langle \mathbf{n}(\mathbf{x}) \rangle \neq 0$. We will detect this spectrum via correlations of the staggered vector spin chirality

$$B_\mu = \epsilon_{\mu\nu\lambda}\partial_\nu A_\lambda = \tfrac{1}{4}\epsilon_{\mu\nu\lambda}\mathbf{n} \cdot (\partial_\nu \mathbf{n} \times \partial_\lambda \mathbf{n}) ; \qquad (3)$$

the last term specifies how B_μ can be related to the operators of the underlying antiferromagnet, and identifies it as the Skyrmion current: the spatial integral of its temporal component B_t is the Skyrmion number of the texture of the Néel order parameter underlining the topological nature of the vector boson. Indeed, correlations of $\epsilon_{\mu\nu\lambda}\mathbf{n} \cdot (\partial_\nu \mathbf{n} \times \partial_\lambda \mathbf{n})$ were measured recently by Fritz *et al.* [21] in quantum Monte Carlo. They can also be measured in Raman scattering [22, 23] if the light couples preferentially to one sublattice of the antiferromagnet.

In the vicinity of a deconfined critical point, we show that the existence of an emergent gauge field implies that the correlations of B_μ obey the universal scaling form

$$\left\langle B_\mu(-p)B_\nu(p) \right\rangle = \left(\delta_{\mu\nu} - \frac{p_\mu p_\nu}{p^2} \right) \rho_s \, \mathcal{F}(p/\rho_s), \qquad (4)$$

where p is a Euclidean 3-momentum, ρ_s is the 'spin stiffness' (or 'helicity modulus') of the Néel phase, and $\mathcal{F}$ is a completely universal scaling function (including its overall scale).
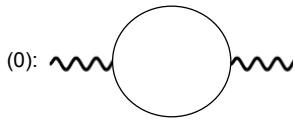
FIG. 1: $N \to \infty$ contribution to the gauge propagator that generates purely dissipative dynamics by decaying into two complex Goldstone bosons leading to Eq. (5). Wiggly line refers to the gauge field and the solid line the N complex Goldstone bosons π.

The stiffness vanishes as $\rho_s \sim (g - g_c)^\nu$ upon approaching the deconfined critical point, where ν is the correlation length exponent. We also note that ρ_s is analogous to the f^2 constant of the chiral Lagriangian of particle physics. Here, ρ_s serves as the low energy scale controlling the excitations of the Néel phase.

The correlator in Eq. (4) is purely transverse; lattice models will also have a longitudinal component, but this is suppressed near the deconfined critical point. In contrast, for a conventional critical point, the longitudinal and transverse components both vanish rapidly with the same large power $\sim \rho_s^{2\Delta_B - 3}$ (and non-universal prefactor), where [21] $\Delta_B \sim 3.4$ is the scaling dimension of the staggered spin chirality (compare to the linear $\sim \rho_s$ power in Eq. (4)).

This paper will obtain numerous properties of the scaling function $\mathcal{F}$ for the deconfined critical point in the $1/N$ expansion. It is useful to first present the form of these gauge-field correlators in the large N limit. After continuing the result to Lorentzian frequencies at zero spatial momentum ($p \to -i\omega$) we have

$$\rho_s \mathcal{F} (\omega/\rho_s) = \frac{1}{N} \frac{-16\omega^2}{(-i\omega + 64\rho_s/N)}; \qquad (5)$$

note that the large N limit is taken with ρ_s/N fixed. This pole in the lower-half of the complex frequency plane at $\omega = -i64\rho_s/N$, arising from the rapid decay due to spin-wave emission (cf. Fig. 1), represents the overdamped vector boson excitation. The large N status of the vector boson is therefore similar to that of the Higgs boson in the Néel phase [7]. And just as was the case for the Higgs boson, we will find here that $1/N$ corrections lead to a non-zero real part in the position of the vector boson pole (see Eq. (9) below), so that at small N we expect that the real and imaginary parts are both of order ρ_s. Moreover, the imaginary part of $\mathcal{F}$ on the real frequency axis, shown in Fig. 3, displays a vector boson resonance for the physically relevant N.

The tensor structure of the vector boson correlator, along with spontaneously broken gauge symmetry in a Higgs phase, represented significant technical obstacles, making this computation more challenging than previous computations of critical properties in the $1/N$ expansion.

We now outline our computation. First, without loss of generality, we choose the z_α condensate along the flavor index $\alpha = 1$ direction, and parameterize $z(x) = \left(\sigma(x)e^{i\omega(x)}, \pi_1(x), \pi_2(x), \ldots, \pi_{N-1}(x)\right)$ where the π_i-fields are complex-valued and $\sigma(x)$ and $\omega(x)$ are real-valued. It is con-

venient to use a radial coordinate system for the first flavor component so that the N-component. As a consequence of this coordinate transformation, the measure of the functional integral for the first flavor component at each point x picks up a Jacobian, $\det J = \sigma$ [24]. In unitary gauge, the (redundant) local gauge transformation function is chosen as the phase variable of the first flavor $\omega(x)$ [24, 25]. Then, as usual, the Goldstone boson of the first flavor is "eaten up" and the action does not depend on $\omega(x)$ anymore. In the large N limit, we find a saddle point with $\sigma = \sqrt{N}\sigma_0$ with $\sigma_0^2 = 1/g - \int_p 1/p^2$. For the amplitude fluctuations around this condensate, we shift $\sigma \to \sqrt{N}\sigma_0 + \sigma$. It is crucial to perform the shift in σ also for the Jacobian, and re-exponentiate it as a propagator $\langle \bar{c}c \rangle$ of fermionic ghost fields $\bar{c}, c$. Note that the inclusion of ghost tadpole diagrams is crucial to ensure that the mass of the Goldstone bosons (π_i's) stays identically zero [26].

We now perform the large-N expansion [27]. The Feynman rules for the various vertices can be obtained from the original action Eq. (1) after the previously mentioned substitutions of the z-fields. We then integrate out the complex Goldstone fields $\pi, \bar{\pi}$ and expand the still dynamical determinant to quadratic order in the fields A_μ, σ and λ [28]. This yields the form of the $N \to \infty$ propagators $\langle \sigma\sigma \rangle$, $\langle \lambda\lambda \rangle$, $\langle \sigma\lambda \rangle$ and $\langle A_\mu A_\nu \rangle$. The gauge field and Lagrange multiplier become dynamical in this way. We then evaluate Wick's theorem keeping all contributions to order $1/N$ after performing the internal flavor trace. Our result for the self-energy of the gauge bosons are the 12 diagrammatic contractions shown in Fig. 2, denoted by

$$\Sigma_{\mu\nu}(p) = \sum_{i=1}^{12} a_i \Sigma_{\mu\nu}^{(i)}(p) , \qquad (6)$$

where we have separated equivalent contractions into numerical factors a_i. The explicit expressions are given in the Supplemental Material. In the past, a reliable evaluation of such tensor-valued Feynman diagrams in momentum space for vectorial correlation functions has been almost intractable. Already for the much simpler case of the (conformally invariant) fixed point of the $O(N)$ vector model, a computation of vectorial correlation functions to $1/N$ is an intricate matter, necessitating the use of conformal field theory methods in real space [29–32]. In momentum space, Cha *et al.* [33] have succeeded to compute the current-current correlator of the $O(N)$ model to $1/N$ but needed to supplement their calculation with results from other computations; and their method seems hard to generalize to more complicated situations.

From a technical viewpoint, the enabling achievement of this paper is the reliable, numerically verifiable computation of tensor-valued momentum integral of multi-loop diagrams using our algorithm Tensoria [26] (see Refs. 34, 35 for an application of similar methods to three-point functions of conformal field theories).

Including the 12 contractions of Fig. 2, we write the renor-
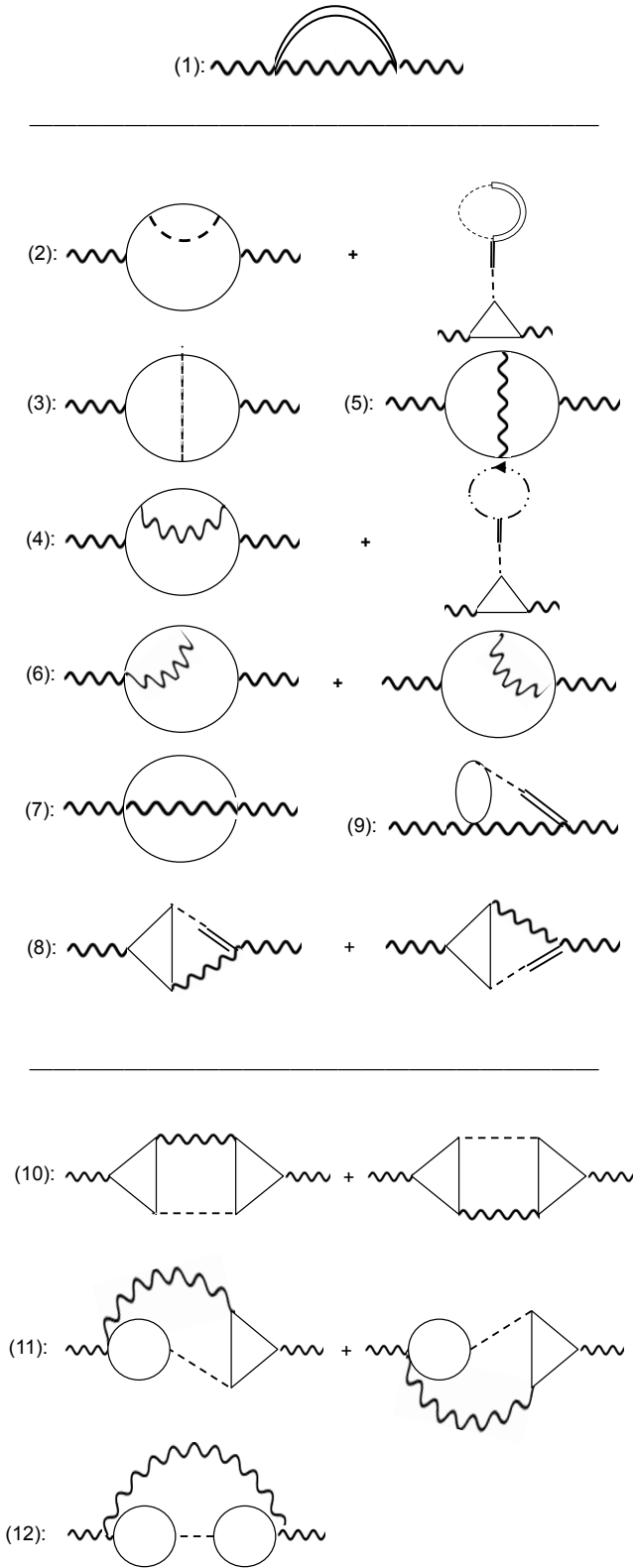
FIG. 2: 1-, 2- and 3-loop diagrams that renormalize the gauge propagator to order $1/N$ after performing the flavor trace. Conventions as in Fig. 1, the double line represents the longitudinal σ field, the dotted line represents the Lagrange multiplier λ field, and the dot-dashed line the fermionic ghost field c. The analytic expressions including factors are given in the Supplemental Material.

malized gauge propagator $D_{\mu\nu}(p) = N\langle A_\mu(-p)A_\nu(p)\rangle$ as

$$\left[D_{\mu\nu}(p)\right]^{-1} = \left(1 - \frac{1}{N}\right)\frac{p}{16}\left(\delta_{\mu\nu} - \frac{p_\mu p_\nu}{p^2}\right) + 2\sigma_0^2\delta_{\mu\nu} - \Sigma_{\mu\nu}(p),$$

(7)

where the terms not proportional to $1/N$ are in fact the $N \to \infty$ contribution shown in Fig. 1 that give the gauge boson its dynamics in the first place.

Before describing the $1/N$-corrections further, we note here that our calculations passed several consistency checks. First of all, we have checked by explicit computation that all diagrams that, individually, would generate a mass for the Goldstone bosons, instead cancel with each other. Moreover, we have computed the correlation length exponent $\nu = 1 - 48/(N\pi^2)$ in agreement with previous work [36, 37] by summing the prefactors of all logarithmic singularities $\sim \log[\Lambda/\sigma_0]\sigma_0^2$ (where Λ is a momentum cutoff) appearing in the 12 self-energy diagrams of Fig. 2. Finally, we computed the gauge field propagator and the current-current correlator also at the critical point (for $\sigma_0 = 0$) [26] and showed in particular that all (logarithmic and other) singularities as a function of momentum p cancel with each other. Thereby, we demonstrated that, as expected [38, 39], these conserved quantities do not pick up anomalous dimensions (beyond the $N \to \infty$ renormalization which is essentially a dimensional effect), and that they fulfill the expected Ward identities between self-energy and vertex corrections.

We now present our main quantitative results for the quantum dynamics of the vector gauge boson in the vicinity of the critical point. As announced earlier, we will compute the position of the pole of the gauge-field propagator on the real frequency axis at zero spatial momentum, and the spectral function which can also be extracted in numerical simulations as well as potentially in experiments. In the large N limit, the pole of the gauge-field propagator (zero in the transverse component of Eq. (7)) is located at $-32\sigma_0^2$, or $\omega = -32\sigma_0^2 i$ in frequency with the Lorentzian time signature, corresponding to an overdamped mode of purely dissipative character. This is just the well known consequence of the decay of the gauge boson into the "particle and anti-particle" continuum of Goldstone bosons (as per Fig. 1) with the scale $32\sigma_0^2$ provided by the Higgs mechanism.

However, after accounting for the self-energy induced shifts of the pole position to $1/N$, the quantum dynamics of the gauge field changes qualitatively and gains an oscillatory response characteristic of a finite lifetime excitation similar to the scattering resonances of the W- and Z boson in particle physics. To determine the shift, the $\Sigma_{\mu\nu}(p)$ integral is calculated at $p = -32\sigma_0^2$ numerically, as described in Ref. 7, by analytically continuing the contour integral. We take $k \to ke^{i\theta}$ and $p \to pe^{i\theta}$, then take the limit of $\theta \searrow -\pi$, rotating the contour around the lower half plane. The θ variation is done gradually, to ensure that we do not cross any poles. For a few of the diagrams, the integral can be done analytically by putting p and k right below the negative real axis, and the analytic and numerical results agree.
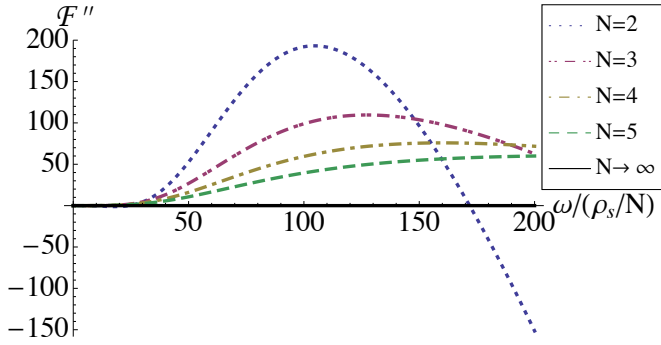
FIG. 3: (Color online) Spectrum of the vector boson as obtained from Eqs. (10, 11) as a function of real frequencies ω at zero spatial momenta displaying the vector boson resonance (in a quantum spin system near a deconfined quantum critical point) as N approaches physically relevant values toward $N = 2$ (blue, dotted curve); the change in sign for large ω at $N = 2$ is due to the breakdown of the $1/N$ expansion, as in Ref. [7]. Frequencies are given in units of the spin stiffness ρ_s, Eq. (8) plotted for $C = 0$. Shifting C away from 0 does not qualitatively change the curves.

Finally, the universal structure of the pole position is revealed by writing σ_0^2 in terms of the spin stiffness ρ_s; their relationship is easily computed at $N = \infty$, and using the scaling law $\rho_s \sim (g - g_c)^\nu$ and the value of ν quoted above, we obtain at order $1/N$

$$\rho_s = \frac{N\sigma_0^2}{2}\left(1 + \frac{48}{N\pi^2}\ln\left(\frac{\Lambda}{32\sigma_0^2}\right) + \frac{C}{N}\right), \qquad (8)$$

where C is a constant of order unity. Then, in terms of Lorentzian frequencies ω, the pole is at

$$\frac{\omega_{\text{pole}}}{\rho_s/N} = -64i + \frac{32}{N}[7.319 - (11.191 - 2C)i] + O(1/N^2). \quad (9)$$

In order to calculate the vector boson spectral function, we expand the renormalized propagator, Eq. (7), to order $1/N$ by $D_{\mu\nu}(p) = D_{\mu\nu}^0(p) + D_{\mu\nu}^0(p)\Sigma_{\mu\nu}^{1/N}(p)D_{\mu\nu}^0(p)$, and write

$$D_{\mu\nu}(p) = H_T(p)\left(\delta_{\mu\nu} - \frac{p_\mu p_\nu}{p^2}\right) + H_L(p)\frac{p_\mu p_\nu}{p^2}. \qquad (10)$$

The transverse part determines the response in Eq. (4), $\rho_s\mathcal{F}(p/\rho_s) = (p^2/N)H_T(p)$, and its imaginary part

$$\mathcal{F}''(\omega/\rho_s) \equiv \frac{1}{\rho_s}\text{Im}\left[\frac{p^2}{N}H_T(p)\Big|_{p\to-i\omega}\right] \qquad (11)$$

determines the spectral properties of the vector boson. The Wick rotation of H_T to real frequencies has to be done numerically similarly to the procedure described above Eq. (9) except that now we rotate directly onto the imaginary axis at $\theta \searrow -\pi/2$.

As can be observed from Fig. 3, the vector boson spectrum at $N \to \infty$ displays a suppressed, broad continuum indicative of the dissipative nature of the vector boson at that order.

For the physically relevant smaller values of N, a peak-like structure emerges, which becomes progressively better defined upon approaching the case $N = 2$ for deconfined quantum magnets. This indicates an enhanced lifetime of the vector boson. In real-time experiments, the vector boson response is that of a damped oscillator. As with the Higgs mode close to the superfluid-to-Mott insulator quantum phase transition [7, 8, 10], we expect this emergent vector boson "resonance" for smaller N to be observable in direct numerical simulations of $SU(N)$ quantum spin models [17, 40] using the observables of Ref. [21], and potentially also in experiments.

* Electronic address: yejinhuh@fas.harvard.edu
[1] L. Balents, Nature **464**, 199 (2010); S. Sachdev, Nature Physics **4**, 173 (2008).
[2] T.-H. Han, J. S. Helton, S. Chu, D. G. Nocera, J. A. Rodriguez-Rivera, C. Broholm, and Y. S. Lee, Nature **492**, 406 (2012).
[3] H. C. Jiang, Z. Wang, and L. Balents, Nature Physics **8**, 902 (2012).
[4] S. Depenbrock, I.P. McCulloch, and U. Schollwöck, Phys. Rev. Lett. **109**, 067201 (2012).
[5] A.W. Sandvik, Phys. Rev. Lett. **98**, 227202 (2007).
[6] T. Senthil, L. Balents, S. Sachdev, A. Vishwanath, and M. P. A. Fisher, Science **303**, 1490 (2004).
[7] D. Podolsky and S. Sachdev, Phys. Rev. B **86**, 054508 (2012).
[8] M. Endres, T. Fukuhara, D. Pekker, M. Cheneau, P. Schauß, C. Gross, E. Demler, S. Kuhr, and I. Bloch, Nature **487**, 454 (2012).
[9] S. Gazit, D. Podolsky, and A. Auerbach, Phys. Rev. Lett. **110**, 140401 (2013).
[10] K. Chen, L. Liu, Y. Deng, L. Pollet, and N. Prokof'ev, Phys. Rev. Lett. **110**, 170403 (2013).
[11] A. W. Sandvik, V. N. Kotov, and O. P. Sushkov, Phys. Rev. Lett. **106**, 207203 (2011).
[12] A. Nahum, J. T. Chalker, P. Serna, M. Ortuño, and A. M. Somoza, Phys. Rev. Lett. **107**, 110601 (2011).
[13] K. Chen, Y. Huang, Y. Deng, A. B. Kuklov, N. V. Prokof ev, and B. V. Svistunov, Phys. Rev. Lett. **110**, 185701 (2013).
[14] Z. Zhu, D. A. Huse, and S. R. White Phys. Rev. Lett. **110**, 127205 (2013).
[15] R. Ganesh, Jeroen van den Brink, and Satoshi Nishimoto, Phys. Rev. Lett. **110**, 127203 (2013).
[16] K. Damle, F. Alet, and S. Pujari, arXiv:1302.1408 (2013).
[17] M. S. Block, R. G. Melko, and R. K. Kaul, arXiv:1307.0519 (2013).
[18] B. Bergerhoff, F. Freire, D. F. Litim, S. Lola, and C. Wetterich,

Phys. Rev. B **53**, 5734 (1996).

[19] L. Bartosch, arXiv:1307.3276 (2013).

[20] N. Read and S. Sachdev, Phys. Rev. B **42**, 4568 (1990).

[21] L. Fritz, R. L. Doretto, S. Wessel, S. Wenzel, S. Burdin, and M. Vojta, Phys. Rev. B **83**, 174416 (2011); Shinya Yasuda and Synge Todo arXiv:1307.4529.

[22] B. S. Shastry and B. I. Shraiman, Phys. Rev. Lett. **65**, 1068 (1990).

[23] N. Nagaosa and P. A. Lee, Phys. Rev. B **43**, 1233 (1991).

[24] G. Münster and E. E. Scholz, Eur. Phys. J. C **32**, 261-268 (2004).

[25] T. Appelquist, J. Carrazone, T. Goldman, and H. R. Quinn, Phys. Rev. D **8**, 1747 (1973).

[26] Y. Huh, P. Strack, and S. Sachdev, arXiv:XXXX.XXXX (2013).

[27] A. M. Polyakov, *Gauge Fields and Strings*, Harwood Academic Publishers (1987).

[28] R. K. Kaul and S. Sachdev, Phys. Rev. B **77**, 155105 (2008).

[29] H. Osborn, and A. Petkou, Ann. Phys. **231**, 311 (1994).

[30] A. C. Petkou, Phys. Lett. B **359**, 101 (1995).

[31] A. Petkou, Ann. Phys. **249**, 180 (1996).

[32] J. Erdmenger, and H. Osborn, Nuclear Phys. B **484**, 431 (1997).

[33] M. C. Cha, M. P. A. Fisher, S. M. Girvin, M. Wallin, and A. P. Young, Phys. Rev. B **44**, 6883 (1991).

[34] A. Bzowski, P. McFadden, and K. Skenderis, JHEP **03**, 091 (2012).

[35] D. Chowdhury, S. Raju, S. Sachdev, A. Singh, and P. Strack, Phys. Rev. B **87**, 085138 (2013).

[36] B. I. Halperin, T. C. Lubensky, and S. -K. Ma, Phys. Rev. Lett. **32**, 292 (1974).

[37] V. Yu. Irkhin, A. A. Katanin, and M. I. Katsnelson, Phys. Rev. B **54** 11953 (1996).

[38] D. Gross, in *Methods in Field Theory*, edited by R. Balian and J. Zinn-Justin (North-Holland, Les Houches, 1975).

[39] M. Franz, T. Pereg-Barnea, D. E. Sheehy, and Z. Tesanovic, Phys. Rev. B **68**, 024508 (2003).

[40] R. K. Kaul, and A. W. Sandvik, Phys. Rev. Lett. **108**, 137201 (2012).

Supplemental Material

The self energy correction at order $1/N$ is a sum over 12 diagrams $\Sigma_{\mu\nu}(p) = \sum_{i=1}^{12} a_i \Sigma_{\mu\nu}^{(i)}(p)$, where the a_i are symmetry and multiplicity factors for each diagram not directly contained in the vertices and propagator Feynman rules. Before the momentum integrations, the expressions for each of the diagrams are

$$\Sigma_{\mu\nu}^{(1)}(p) = \frac{32\sigma_0^2}{N} \int_q \left(\delta_{\mu\nu} + \frac{q_\mu q_\nu}{32q\sigma_0^2} \right) \frac{1}{(q + 32\sigma_0^2)|p+q|(|p+q| + 16\sigma_0^2)} \qquad a_1 = 4$$

$$\Sigma_{\mu\nu}^{(2)}(p) = -\frac{8}{N} \int_q \int_k \frac{(2k+p)_\mu(2k+p)_\nu q^2}{k^4(p+k)^2(q+16\sigma_0^2)} \left(\frac{1}{(k+q)^2} - \frac{1}{q^2} \right) \qquad a_2 = 2$$

$$\Sigma_{\mu\nu}^{(3)}(p) = -\frac{8}{N} \int_q \int_k \frac{(2k+p)_\mu(2(k+q)+p)_\nu q^2}{k^2(p+k)^2(k+q)^2(p+k+q)^2(q+16\sigma_0^2)} \qquad a_3 = 1$$

$$\Sigma_{\mu\nu}^{(4)}(p) = \frac{16}{N} \int_q \int_k \frac{(2k+p)_\mu(2k+p)_\nu}{k^4(p+k)^2(q+32\sigma_0^2)} \left(\frac{(2k+q)_\lambda(2k+q)_\rho}{(k+q)^2} - \frac{q_\lambda q_\rho}{q^2} \right) \left(\delta_{\lambda\rho} + \frac{q_\lambda q_\rho}{32q\sigma_0^2} \right) \qquad a_4 = 2$$

$$\Sigma_{\mu\nu}^{(5)}(p) = \frac{16}{N} \int_q \int_k \frac{(2k+p)_\mu(2(k+q)+p)_\nu(2(k+p)+q)_\lambda(2k+q)_\rho}{k^2(p+k)^2(k+p+q)^2(k+q)^2(q+32\sigma_0^2)} \left(\delta_{\lambda\rho} + \frac{q_\lambda q_\rho}{32q\sigma_0^2} \right) \qquad a_5 = 1$$

$$\Sigma_{\mu\nu}^{(6)}(p) = -\frac{16}{N} \int_q \int_k \frac{(2k+q)_\rho(2k+p)_\nu}{k^2(k+q)^2(k+p)^2(q+32\sigma_0^2)} \left(\delta_{\lambda\rho} + \frac{q_\lambda q_\rho}{32q\sigma_0^2} \right) \delta_{\mu\lambda} + (\mu \leftrightarrow \nu) \qquad a_6 = 4$$

$$\Sigma_{\mu\nu}^{(7)}(p) = \frac{16}{N} \int_q \int_k \frac{1}{(k+q)^2(k+p)^2(q+32\sigma_0^2)} \left(\delta_{\lambda\rho} + \frac{q_\lambda q_\rho}{32q\sigma_0^2} \right) \delta_{\mu\lambda} \delta_{\nu\rho} \qquad a_7 = 4$$

$$\Sigma_{\mu\nu}^{(8)}(p) = \frac{256}{N} \int_q \int_k \left(\frac{(2k+p)_\mu(2k+2p+q)_\lambda}{k^2(k+p)^2(k+p+q)^2} + \frac{(2k+p)_\mu(2k-q)_\lambda}{k^2(k+p)^2(k-q)^2} \right) \frac{\sigma_0^2 \delta_{\rho\nu}}{(|p+q| + 16\sigma_0^2)(q+32\sigma_0^2)} \left(\delta_{\lambda\rho} + \frac{q_\lambda q_\rho}{32q\sigma_0^2} \right) \qquad a_8 = 2$$

$$\Sigma_{\mu\nu}^{(9)}(p) = -\frac{256\sigma_0^2}{N} \int_q \int_k \frac{1}{k^2(k+p+q)^2} \frac{1}{(|p+q| + 16\sigma_0^2)(q+32\sigma_0^2)} \left(\delta_{\mu\nu} + \frac{q_\mu q_\nu}{32q\sigma_0^2} \right) \qquad a_9 = 4$$

$$\Sigma_{\mu\nu}^{(10)}(p) = -\frac{128}{N} \int_{q,k,l} \left[\frac{(2k+p)_\mu(2k+q)_\lambda}{k^2(k+p)^2(k+q)^2} \frac{(2l+q)_\rho(2l+p)_\nu}{l^2(l+p)^2(l+q)^2} \frac{(p-q)^2}{(|p-q| + 16\sigma_0^2)(q+32\sigma_0^2)} \left(\delta_{\lambda\rho} + \frac{q_\lambda q_\rho}{32q\sigma_0^2} \right) \right.$$
$$\left. + \frac{(2k+p)_\mu(2k+p+q)_\lambda}{k^2(k+p)^2(k+q)^2} \frac{(2l+p+q)_\rho(2l+p)_\nu}{l^2(l+p)^2(l+q)^2} \frac{q^2}{(q+16\sigma_0^2)(|p-q| + 32\sigma_0^2)} \left(\delta_{\lambda\rho} + \frac{(p-q)_\lambda(p-q)_\rho}{32|p-q|\sigma_0^2} \right) \right] \qquad a_{10} = 2$$

$$\Sigma_{\mu\nu}^{(11)}(p) = \frac{128}{N} \int_{q,k,l} \left[\frac{\delta_{\mu\lambda}}{k^2(k+p+q)^2} \left(\frac{(2l-q)_\rho(2l+p)_\nu}{l^2(l-q)^2(l+p)^2} + \frac{(2l+2p+q)_\rho(2l+p)_\nu}{l^2(l+p)^2(l+p+q)^2} \right) \times \right.$$
$$\left. \frac{(p+q)^2}{(q+32\sigma_0^2)(|p+q| + 16\sigma_0^2)} \left(\delta_{\lambda\rho} + \frac{q_\lambda q_\rho}{32q\sigma_0^2} \right) \right] \qquad a_{11} = 4$$

$$\Sigma_{\mu\nu}^{(12)}(p) = -\frac{128}{N} \int_{q,k,l} \frac{1}{k^2(k+p+q)^2} \frac{1}{l^2(l+p+q)^2} \frac{(p+q)^2}{(|p+q| + 16\sigma_0^2)(q+32\sigma_0^2)} \left(\delta_{\mu\nu} + \frac{q_\mu q_\nu}{32q\sigma_0^2} \right) \qquad a_{12} = 4.$$

$$(12)$$

These integrals can be evaluated using our algorithm Tensoria as described in the text and in Ref. 26. To extract the critical exponent ν from the logarithmic singularity and evaluate the finite terms to determine the pole position and spectral function, we pull out the momentum cutoff (Λ) dependent part and split the rest into transversal and longitudinal components:

$$\Sigma_{\mu\nu}^{(i)}(p) = \frac{1}{N} \left[I_T^{(i)}(p) \left(\delta_{\mu\nu} - \frac{p_\mu p_\nu}{p^2} \right) + I_L^{(i)}(p) \frac{p_\mu p_\nu}{p^2} \right] + \frac{1}{N} \left[\frac{14\Lambda}{3\pi^2} - \frac{96\sigma_0^2}{\pi^2} \log \frac{\Lambda}{32\sigma_0^2} \right] \delta_{\mu\nu} . \qquad (13)$$

Here the term proportional to Λ is a consequence of the non-gauge-invariant momentum cutoff, but can be safely absorbed into a shift in the position of the critical point; such artifacts do not propagate to the universal constants computed here, which are gauge invariant. The logarithmic singularity yields the correlation length $\nu = 1 - 48/(N\pi^2)$ described in the main text, and is absorbed after σ_0^2 is expressed in terms of ρ_s via Eq. (8). For the remaining part, we evaluate the analytically continued pole contributions at the location of the $N \to \infty$ pole position ($p = -32\sigma_0^2$). The numerical integration yield to high accuracy (all

constants below are in units of σ_0^2)

$$
\begin{array}{ll}
I_T^{(1)} = -2.882 - 0.374i & I_L^{(1)} = -0.213 + 0.246i \\
I_T^{(2)} = -0.548 - 0.265i & I_L^{(2)} = -0.270 + 0.318i \\
I_T^{(3)} = 0.539 + 1.197i & I_L^{(3)} = 0 + 0.098i \\
I_T^{(4)} = 0.476 + 0i & I_L^{(4)} = -0.050 + 0i \\
I_T^{(5)} = 1.895 - 0.587i & I_L^{(5)} = -0.994 + 0i \\
I_T^{(6)} = -0.454 + 0i & I_L^{(6)} = 0.548 + 0i \\
I_T^{(7)} = -1.754 + 0i & I_L^{(7)} = -0.274 + 0i \\
I_T^{(8)} = -0.629 - 0.148i & I_L^{(8)} = -0.426 + 0.492i \\
I_T^{(9)} = 2.882 + 0.374i & I_L^{(9)} = 0.213 - 0.246i \\
I_T^{(10)} = -0.606 - 3.098i & I_L^{(10)} = -0.635 + 0.492i \\
I_T^{(11)} = 1.083 + 0.148i & I_L^{(11)} = -0.121 - 0.492i \\
I_T^{(12)} = -1.128 - 0.374i & I_L^{(12)} = 0.061 + 0.246i \ .
\end{array}
\tag{14}
$$

Combining these, we get

$$
\begin{aligned}
I_T^{tot} &= \sum_i a_i I_T^{(i)} = -9.191 - 7.319i \\
I_L^{tot} &= \sum_i a_i I_L^{(i)} = -2.906 + 1.720i \ .
\end{aligned}
\tag{15}
$$